THE JOURNAL OF PHYSICAL CHEMISTRY B

Article

pubs.acs.org/JPCB

Use of Dielectric Spectroscopy To Monitor Molecular Mobility in Glassy and Supercooled Trehalose

Sunny P. Bhardwaj and Raj Suryanarayanan*

Department of Pharmaceutics, University of Minnesota, Minneapolis, Minnesota 55455, United States

ABSTRACT: Dielectric spectroscopy was used to comprehensively characterize the molecular mobility in amorphous trehalose, an extensively used bioprotective agent. Isothermal frequency sweeps were carried out at different temperatures in the glassy and supercooled liquid states of freeze-dried trehalose. Two previously reported secondary relaxations were observed at temperatures far below its glass transition temperature (T_g). At temperatures close to T_g, removal of dc conductivity contribution revealed a relaxation peak. The origin of this peak was evaluated using several diagnostic tests and determined to be the α-relaxation. There was also an excess wing in the high-frequency tail of α-relaxation. Sub-T_g annealing caused the primary relaxation to shift to lower frequencies, enabling resolution of the excess wing, which was characterized to be the true Johari–Goldstein (JG) relaxation. A qualitatively similar effect of annealing on JG relaxation was also observed. The average relaxation times of the two previously reported secondary relaxations were unaffected by annealing.

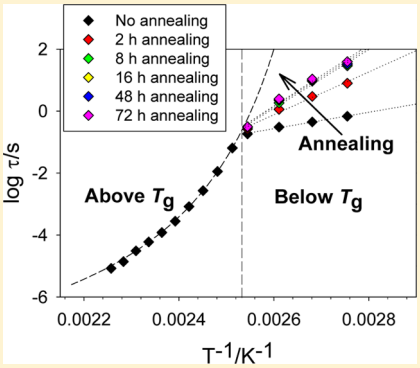

INTRODUCTION

Trehalose (α-D-glucopyranosyl α-D-glucopyranoside) is a nonreducing disaccharide made up of two glucose units. It serves as a "bioprotective" in many anhydrobiotic organisms which can survive desiccation stress by internally accumulating this sugar. Trehalose is also extensively used as a stabilizer of biomolecules such as proteins and phospholipids.[1,2] A high glass transition temperature (~117 °C) coupled with its resistance to crystallization confers a unique status to this disaccharide. However, its crystallization during freeze-drying has recently been reported.[3,4] Since the ability of trehalose to serve as a stabilizer hinges on its existence in the amorphous state,[5] there is an urgent need to comprehensively investigate its crystallization behavior.

Molecular mobility has often been proposed to be the major factor governing the physical and chemical instability of amorphous compounds. Many investigations have shown a correlation between molecular mobility and physical stability of amorphous materials.[6−8] In such instances, reduction in molecular mobility will be an effective approach to increase physical stability. Mobility can be influenced either by reducing the storage temperature or by the inclusion of an additive. Molecular mobility encompasses both global and local motions. Global mobility, reflecting cooperative molecular motions, is responsible for the glass transition phenomenon and is also known as primary, structural, or α-relaxation. The α-relaxation has often been considered the major determinant of the physical stability in the amorphous state. On the other hand, fast noncooperative motions either emanating from a part of a molecule or involving a complete molecule are termed local.[9−11] These local motions are also referred to as secondary or β-relaxations and there is increasing evidence of their influence on the physical instability of amorphous state. Two observations indirectly implicate the role of local mobility: (i) the lack of correlation between crystallization propensity and structural relaxation time, and (ii) crystallization at temperatures substantially below T_g.[12−15] Out of several secondary relaxations, the Johari–Goldstein (JG) relaxation has been extensively investigated.[16,17] Although the origin of this relaxation is not fully understood, it is thought to involve the motion of the entire molecule. The JG relaxation is not only considered to influence stability but is also believed to be the precursor to global mobility.[18,19]

Several techniques, including differential scanning calorimetry (DSC),[20,21] dielectric spectroscopy,[6,7] shear viscosity measurement,[22] and nuclear magnetic relaxation time measurement,[8,23] have been used to study molecular mobility in the amorphous state. Out of these, dynamic dielectric spectroscopy (DDS) is an important tool which can distinguish between different modes of mobility. It confers the ability to comprehensively "map" different relaxations in a variety of amorphous materials.[13,24] Molecular mobility investigations in trehalose, using DDS, have been limited by the considerable interference from dc conductivity.[24−26] This interference is particularly pronounced at temperatures close to T_g. Hence, modulated DSC has been used to estimate its global mobility.[24] Kaminski et al. used the Kramers–Kronig relation to investigate α-relaxation in supercooled trehalose.[25] Recently, while characterizing amorphous trehalose prepared by freeze-drying, we were able to identify and study some new kinetic features.[27,28] Using the Kramers–Kronig transformation, we effectively removed the contribution of dc conductivity thereby

Received: April 6, 2012
Revised: July 6, 2012
Published: August 22, 2012

completely resolving α-relaxation at temperatures below T_g. Additionally, an excess wing was also identified in the high-frequency flank of α-relaxation. By comparing (i) the annealing time dependence of this relaxation peak with α-relaxation and (ii) its average relaxation time with the calculated independent relaxation time, it was demonstrated that the Johari−Goldstein process is responsible for this peak. Earlier, two sub-T_g relaxations, designated as β_1 and β_2 (or as γ and β), were reported in trehalose.[24,25,29] Recently, Kwon et al. also observed an excess wing in amorphous trehalose.[30] They modeled the data with two Cole−Cole (CC) functions, one each for α-relaxation and the "excess" wing, and two Havriliak−Negami functions for the faster secondary relaxations. However, since the contribution of dc conductivity is significant in the lower frequency range where the α-relaxation and excess wing appear, modeling the data without conductivity removal has the potential to lead to erroneous results. Kaminski et al. argued that the peak designated as primary relaxation by Kwon et al. is due to dc conductivity and the excess wing observed by Kwon et al. is the structural relaxation.[31] Thus, there is still lack of consensus regarding the exact nature of the different dielectric relaxations in amorphous trehalose. These observations indicate that a comprehensive characterization of molecular mobility in amorphous trehalose is warranted. In light of the concerns raised by Kaminski et al., it is important to conclusively document the exact origin of the different mobility features in the dielectric spectrum of trehalose.

The potential effect of annealing on the mobility of amorphous compounds is well recognized in the materials science community. However, in case of trehalose, only the effect of short-term annealing (up to 8 h) has been documented in two investigations.[28,29] We had observed a progressive increase in α-relaxation time with annealing.[28] Moreover, the excess wing developed into a partially resolved and hitherto unidentified β-relaxation peak. The objective of our current study is to characterize the "new" Johari−Goldstein relaxation. This is important in light of the potential role of JG relaxation on the physical stability of trehalose. Additionally, the effect of long-term annealing on α-relaxation and secondary relaxation of trehalose is of interest and importance not only to food and pharmaceutical scientists but also to the cryobiology community. The importance of long-term annealing stems from the fact that it could lead to a glassy matrix which is closer to the "equilibrium state". *If this significantly slows down the molecular motions responsible for physicochemical instability, it can be an effective stabilization strategy.* It is noteworthy that trehalose is extensively used to stabilize macromolecules and a long shelf life is a particularly desirable attribute. We have therefore comprehensively mapped the mobility in amorphous trehalose, encompassing α- and several β-relaxations followed by the effect of long-term sub-T_g annealing on these relaxations.

EXPERIMENTAL SECTION

Preparation and Baseline Characterization of Amorphous Trehalose. Trehalose dihydrate ($C_{12}H_{22}O_{11}\cdot 2H_2O$; Sigma, St. Louis, MO; purity >99%) was used as received. Amorphous trehalose was prepared by freeze-drying aqueous trehalose solution (10% w/v) in a benchtop freeze-dryer (Model UNITOP 400 L, Virtis, Gardiner, NY).[28] The powder, in tightly capped glass containers, was stored at −20 °C in a desiccator. In order to minimize water sorption, further handling was done in a glovebox maintained at RH < 5% (RT). Freeze-dried trehalose was X-ray amorphous and the water content <0.5% w/w (determined by Karl Fischer titrimetry and thermogravimetry). The calorimetric T_g (onset temperature) was ∼117 °C.

Dynamic Dielectric Spectroscopy. Isothermal dielectric measurements were carried out using a broadband dielectric spectrometer (Novocontrol Alpha-A high performance frequency analyzer, Novocontrol Technologies, Germany), typically in the frequency range of 10^{-1}−10^7 Hz at various temperatures in the range 25−170 °C. Powder sample was placed in an electrode assembly consisting of two round copper electrodes (20 mm diameter) and a PTFE spacer. Excess powder was filled between the electrodes which were then compressed against each other to ensure that there was complete contact of the sample with the electrode surface. The PTFE spacer (thickness: 1 mm, area: 59.69 mm^2, and capacity: 1.036 pF) enabled sample confinement between electrodes at elevated temperatures and also minimized errors due to stray capacitance or edge effects. Samples of different thickness were analyzed to ensure that, in the frequency region of interest, there was no interference from interfacial polarization. The Havriliak−Negami function (eq 1) was used to fit the dielectric profiles to obtain various relaxation parameters for different relaxations peaks.

$$\varepsilon^*(\omega) = \varepsilon_\infty + \frac{\Delta\varepsilon}{(1 + (i\omega\tau_{HN})^{\beta_{HN}})^{\gamma_{HN}}} \quad (1)$$

$$\varepsilon^*(\omega) = \varepsilon'(\omega) - i\varepsilon''(\omega) \quad (2)$$

where $\varepsilon^*(\omega)$ is the complex dielectric permittivity (eq 2) consisting of dielectric constant (ε') and dielectric loss factor (ε''), ω represents the angular frequency which is equal to $2\pi f$ with f being the frequency in Hz, τ is the relaxation time and dielectric strength, and $\Delta\varepsilon = \varepsilon_s - \varepsilon_\infty$, where ε_s gives the low-frequency limit ($\omega \to 0$) of $\varepsilon'(\omega)$ and ε_∞ is the high-frequency limit ($\omega \to \infty$) of $\varepsilon'(\omega)$. The β_{HN} and γ_{HN} are the shape parameters describing the symmetric and asymmetric peak broadening respectively with $0 < \beta$ (or γ) < 1.

RESULTS AND DISCUSSION

Molecular Mobility in Unannealed Trehalose. *Dielectric Relaxation Behavior at a Fixed Frequency.* The dielectric features due to molecular motions, in the glassy as well as supercooled trehalose, were monitored in an isochronal temperature sweep experiment. Both ε' and ε'' were determined in temperature increments of 5 °C, over the range of 25−180 °C, at a fixed frequency of 1 kHz (Figure 1). Three relaxations were apparent in the investigated temperature range. The calorimetric T_g onset (indicated by an arrow in the Figure 1) was found to coincide with the onset of the major dielectric peak which is characteristic of α-relaxation. Additionally, two secondary relaxations, represented by an extra contribution to the lower temperature region of the α-relaxation and a peak at ∼40 °C, were also observed.

Molecular Mobility in Unannealed Amorphous Trehalose. Isothermal frequency sweep experiments were carried out at various temperatures ranging from room temperature to 170 °C. For each measurement, the frequency range traversed was 10^{-1}−10^7 Hz and the typical measurement time was ∼5 min. This was done to minimize annealing during the experiments at temperatures below T_g as well as to minimize the chemical degradation of amorphous trehalose at high temperatures. Figure 2a shows the dielectric loss spectrum of trehalose at 25 °C. As reported earlier,[24,25,29] two unresolved β-relaxation or

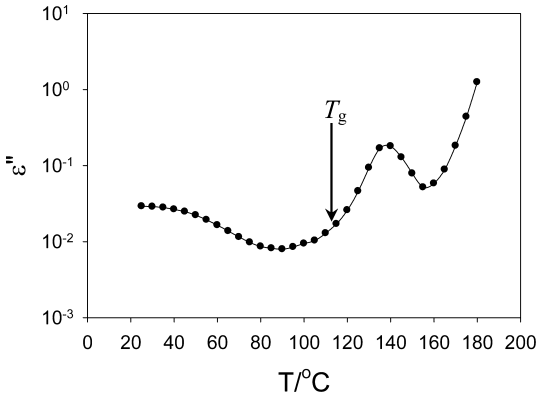

Figure 1. Plot of dielectric loss versus temperature in amorphous trehalose. The calorimetric T_g onset is shown by an arrow.

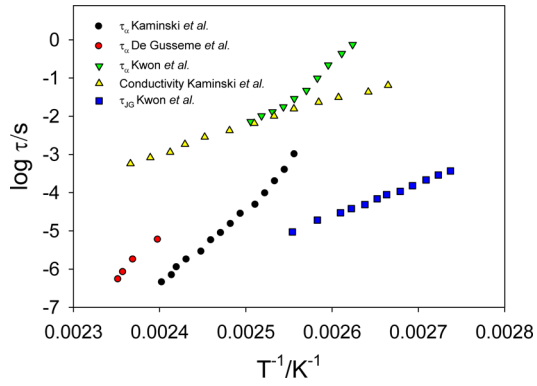

Figure 3. Plots of (i) structural relaxation time (Kaminski et al.,[31] De Gusseme et al.,[24] Kwon et al.[30]), (ii) dc conductivity (Kaminski et al.[31]), and (iii) Johari–Goldstein relaxation time (Kwon et al.[30]) as a function of temperature. The values from different sources were obtained by digitizing the published plots.

secondary relaxation peaks were observed. At this temperature, which is ~90 °C below T_g, relaxation peaks correspond to the local motions in the glassy matrix. The two unresolved β-relaxations were simultaneously fitted using the Havriliak–Negami equation to obtain the average relaxation times as well as other parameters. The faster of the two relaxations is designated as β_1 and the slower as β_2. In agreement with the literature reports,[24,25,29] the dielectric loss and hence dielectric strength of the β_1-relaxation was higher than that of β_2-relaxation. As shown in Figure 2b, both the relaxations shifted to higher frequencies and their dielectric strengths decreased with increasing temperature (a part of the β_1-relaxation is outside the frequency range).

One of the issues with trehalose, as already mentioned, is the interference of dc conductivity. Recently, Kwon et al. recognized the shoulder in the conductivity tail to be the α-relaxation peak and modeled it without dc conductivity removal.[30] Kaminski et al. argued that the relaxation peak, which Kwon et al. labeled as the α-relaxation, originated from dc conductivity and the actual primary relaxation was mislabeled as the excess wing.[31] However, in an effort to perform a careful comparison, we digitized the relevant plots from the literature and present all the data in Figure 3. There is approximately 2 orders of magnitude difference in the values of the average relaxation time reported by Kwon et al. as excess wing (~9.41×10^{-6} s; ~118 °C) and by Kamisnki et al. as structural relaxation (~1.01×10^{-3} s; ~118 °C). Similarly, the structural relaxation times reported by Kaminski et al. and De Gusseme et al. seem to differ by about an order of magnitude at any given temperature (Figure 3). Comparing the relaxation times at 143 °C, they are 5.88×10^{-6} s (De Gusseme) and 4.49×10^{-7} s (Kaminski). These differences were difficult to observe in the earlier publication since the temperature scale was compressed to accommodate numerous relaxation profiles in one figure (Figure 1 in the paper by Kaminski et al.[31]). There are similar differences in the relaxation values reported by different groups for the two local relaxations as well (Figure 1 in the paper by Kaminski et al.[31]). This difference is more pronounced in the case of the slower β-relaxation. Thus, in amorphous trehalose, there seems to be a readily discernible difference in the relaxation time values reported by different groups. Importantly, if the temperature dependence of α-relaxation time reported by Kaminski et al. and De Gusseme et al. is extrapolated to lower temperatures, at temperatures close to T_g, both α-relaxation and conductivity relaxation will have similar relaxation time values (Figure 3). In other words, in this temperature range, structural relaxation will be overshadowed by dc conductivity. This implies that, at temperatures close to T_g, the actual α-relaxation is indeed hidden in the conductivity contribution. In light of potential experimental artifacts, accurate assignment of α-relaxation can be a challenge even when the conductivity contribution is removed. The potential experimental artifacts and the steps taken to address them will be discussed later. However, the first step was to effectively remove the contribution of dc conductivity to the dielectric loss measurements so as to characterize α-relaxation.

Figure 4a shows the relaxation loss spectra of amorphous trehalose at 100, 110, and 120 °C where α-relaxation is barely

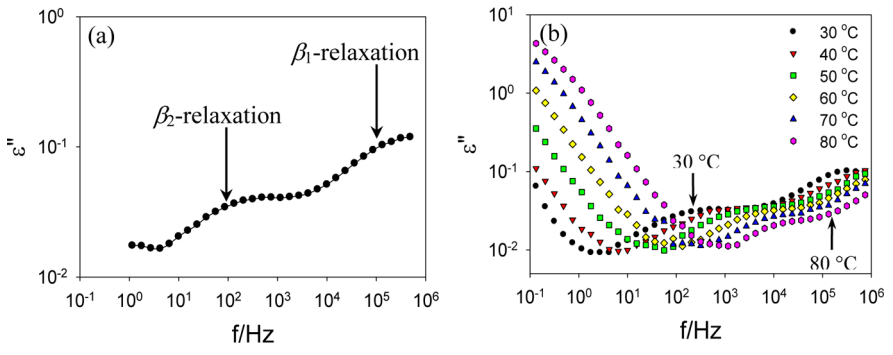

Figure 2. Dielectric loss spectra of amorphous trehalose (a) at 25 °C and (b) over the temperature range of 30–80 °C. Two secondary relaxations are shown.

dx.doi.org/10.1021/jp303317p | J. Phys. Chem. B 2012, 116, 11728–11736

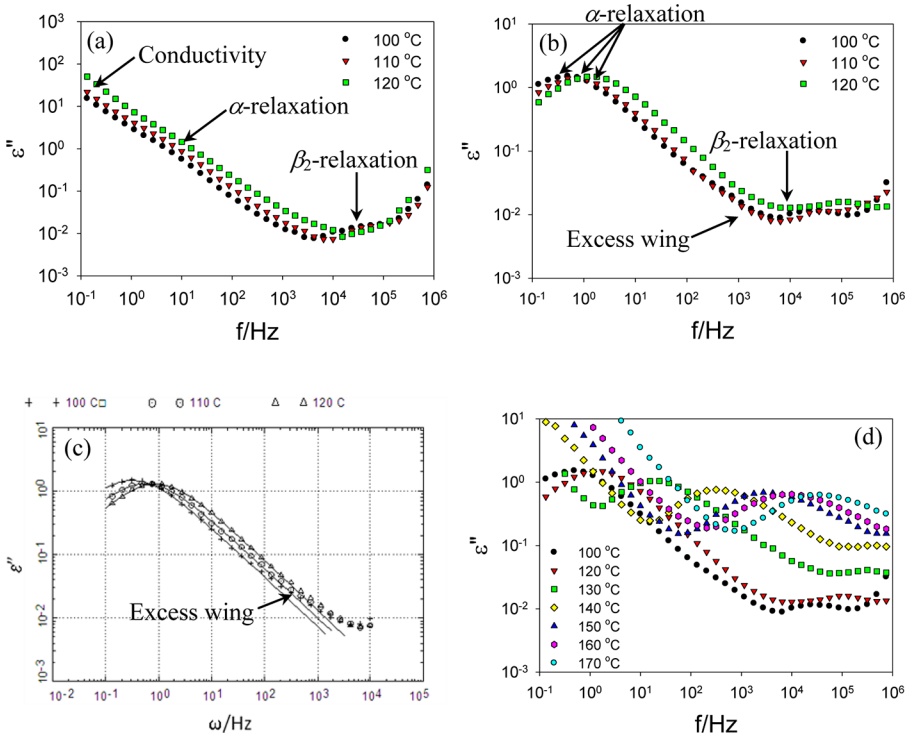

Figure 4. Plots of dielectric loss as a function of frequency for amorphous trehalose at 100, 110, and 120 °C: (a) before dc conductivity removal (α-relaxation visible as a shoulder in the conductivity tail), (b) calculated using the Kramers–Kronig transformation, and (c) showing an excess wing following the modeling of α-relaxation. (d) Plots of dielectric loss as a function of frequency over the temperature range of 100–170 °C. At temperatures ≤140 °C, the contribution of dc conductivity was removed.

discernible due to interference from dc conductivity. As reported earlier, with increasing temperature, there was an increased contribution of dc conductivity at low frequencies.[24,25,30] In order to determine the structural relaxation time close to T_g, we used a derivative method of analysis based on the Kramers–Kronig relation (eq 3).[25,32]

$$\varepsilon'' \approx \frac{\pi}{2}\frac{\varepsilon'(\omega_1) - \varepsilon'(\omega_2)}{\ln\left(\frac{\omega_2}{\omega_1}\right)} \tag{3}$$

It links the imaginary (ε'') and real (ε') permittivity which are parts of the complex dielectric permittivity, ε^*. Since ε' is unaffected by conductivity, it was used to calculate ε'' at different frequencies.[28] Moreover, there was no contribution of interfacial polarization to the permittivity in the frequency range studied and, thus, the dielectric constant has contributions only from the relaxation processes. It is evident from Figure 4 (panels b and d) that once the conductivity contribution was removed, completely resolved α-relaxation peak was observed at temperatures both above and below T_g.

The sources of artifacts, both instrument and sample-related, were systematically considered. The presence of water or air bubbles at the surface of electrodes or the oxidation of metal electrodes could lead to the appearance of Debye-like peaks.[31,33,34] Similar artifact peaks have also been observed when blocking electrode technique has been used to study a relaxation process overlapping with conductivity.[35] In all these cases, the presence of an insulating component is the source of the additional peak. A simple diagnostic feature of this additional peak is that it occurs at a frequency where $\varepsilon' = \varepsilon''$, i.e., the conductivity relaxation frequency.[34] However, if the structural relaxation occurs in the same frequency range, its unambiguous identification and characterization will be challenging. These issues take on special significance in the case of solid powders where there is the possibility of air entrapment or water sorption during sample preparation. To minimize the effects of these experimental artifacts, sample preparation should be done in controlled environmental conditions of very low water vapor pressure. Metal electrodes should be checked for signs of oxidation, particularly when experiments are conducted at elevated temperatures. Replicate analyses and comparison of the peak amplitudes will enable identification of the conductivity peak since the amount of air/water is likely to vary from sample to sample and will affect peak amplitude.[34] If water or air is the source of the conductivity peak, this can be readily identified by subjecting the sample to an elevated temperature. This will result in dissolution/desorption leading to a pronounced decrease in conductivity peak amplitude.[34]

In the case of amorphous trehalose, at temperatures close to T_g, the primary relaxation peak does appear in the same region where ε' and ε'' are equal. As discussed earlier, this is due to the converging temperature dependences of the two processes as presented by Kaminski et al.[31] It was therefore important to check the origin of the peak after Kramers–Kronig transformation. We used a new pair of electrodes for each sample and also visually checked them at the end of the measurement to ensure that there was no oxidation. A lot of effort was expended to minimize the exposure of the amorphous samples to ambient conditions. The sample preparation and handling of the electrode assembly was done in a glovebox maintained at RH < 5% (RT). The water content in all the samples was <0.5% w/w. It is, however, recognized that this very small amount of water could make significant contribution to the

dx.doi.org/10.1021/jp303317p | J. Phys. Chem. B 2012, 116, 11728–11736

observed response. Once the conductivity was subtracted using the Kramers–Kronig transformation, in replicate measurements, the amplitudes of the relaxation peak were extremely reproducible (coefficient of variation <5%), indicating that the observed peak is due to primary relaxation and not conductivity. Further, storage at high temperatures ($>T_g$) did not change the peak amplitude.

The fact that this is indeed the α-relaxation peak was also confirmed by determining its temperature dependence across T_g (discussed later). At temperatures >140 °C, the α-relaxation peak moved to a higher frequency region and was resolved from conductivity. Thus, the conductivity subtraction was no longer necessary and the data could be used "as is". As discussed later, the temperature dependence of the α-relaxation time over the entire supercooled region could be fitted with a single Vogel–Tammann–Fulcher (VTF) model. As this temperature range included both the "dc conductivity subtracted" and the "as-is" data, this again proves that it is the same relaxation process over this entire temperature range.

The average relaxation time and shape parameters for this mobility were determined by fitting the relaxation peak with the Havriliak–Negami model. One unusual observation is the high value of β_{KWW} (~0.83) observed at temperatures close to T_g. However, it must be recognized that the derivative form of Kramers–Kronig relation is an approximation and has the potential to underestimate the distribution of relaxation times (more Debye-like peak).[36] Under conditions where conductivity was no longer contributing to α-relaxation (temperatures >140 °C) and thus no Kramers–Kronig transformation was carried out, the calculated β_{KWW} for the supercooled trehalose was ~0.5. De Gusseme et al., using differential scanning calorimetry, reported a β_{KWW} value of 0.3.[24] Similar differences exist for other sugars; for example, Bhugra et al. and Kaminski et al. reported β_{KWW} values of 0.64 and 0.38, respectively, for supercooled sucrose.[6,37]

The removal of conductivity also revealed a shoulder on the high-frequency tail of α-relaxation peak (Figure 4, panels b and c). This excess wing is a common feature in the dielectric spectra of many amorphous materials and has been shown to be the high-frequency flank of the JG relaxation which is masked by the α-relaxation peak.[38,39] We have shown in a previous report that in the case of glassy trehalose, on annealing, this excess wing also developed into a relaxation peak.[28] In addition to being the slowest secondary relaxation, it was affected by the initial annealing and was therefore attributed to the JG process. Moreover, there was a very good agreement between the relaxation time of this mobility and the calculated independent relaxation times based on the coupling model. The importance of this observation stems from the fact that JG relaxation is considered a universal feature in amorphous materials and a precursor to global mobility. As mentioned earlier, an excess wing was also reported based on the model fitting of the as-is dielectric profile of amorphous trehalose.[30] Since, the dc conductivity appears in the frequency region of both α-relaxation and excess wing, the simultaneous modeling approach could lead to inaccurate results. Further characterization of this excess wing, once it could be partially resolved from the α-relaxation peak, is discussed in detail later.

Temperature Dependence of Different Relaxations. Figure 5 shows the temperature dependence of relaxation times for different mobility modes in amorphous trehalose. The two secondary (β_1 and β_2) relaxations, as expected, exhibited Arrhenius behavior over the experimental temperature range.

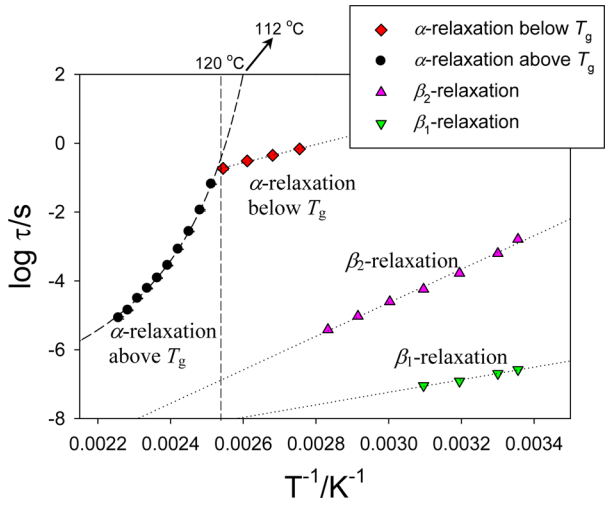

Figure 5. Plots of the temperature dependence of α-, β_1-, and β_2-relaxation times. The dotted lines indicate Arrhenius behavior and the dashed line indicates VTF behavior.

As the temperature was increased toward T_g, these relaxations moved out of the frequency range of the instrument and therefore their temperature dependence was restricted to sub-T_g range. The activation energy for the slower β_2-relaxation (~92 kJ/mol) was higher than that of the faster β_1-relaxation (~34 kJ/mol), in agreement with earlier reports.[24,25] Between the different groups of workers, there is a good agreement in the reported temperature dependence (measured as activation energy) of the secondary relaxations.[24,25,30] However, at any given temperature, there was up to an order of magnitude difference in the absolute value of the slower β_2-relaxation time (Figure 1 in Kaminski et al.[31]). The differences were less pronounced for the faster β_1-relaxation (also called the γ-relaxation). Our results for both these local relaxations are in excellent agreement with those of De Gusseme et al.[24]

The temperature dependence of primary relaxation was studied both below and above T_g. The dielectric loss profiles, over the temperature range of 100–170 °C, are plotted in Figure 4d. In the dielectric profiles obtained above 140 °C, the α-relaxation peak was well separated from conductivity, and therefore no conductivity subtraction was necessary. To rule out crystallization, select samples were subjected to X-ray diffractometry after the DDS run and were observed to be amorphous. As shown in Figure 5, the dielectric T_g of trehalose was ~120 °C, based on the change in the temperature dependence of structural relaxation time. This is in good agreement both with the calorimetric T_g onset of ~117 °C (Experimental Section) and with several literature values of dry trehalose.[40−43] While there was considerable deviation from linearity above T_g, Arrhenius behavior was observed in the narrow temperature range below T_g (Figure 5). This behavior is typical of α-relaxation which shows a pronounced change in temperature dependence across T_g.[44−46] This also proves that the observed mobility is the α-relaxation in amorphous trehalose. The VTF equation is generally used to describe the nonlinear temperature dependence of α-relaxation in the supercooled region (eq 4):

$$\tau(T) = \tau_0 \exp\left(\frac{DT_0}{T - T_0}\right) \quad (4)$$

dx.doi.org/10.1021/jp303317p | J. Phys. Chem. B 2012, 116, 11728–11736

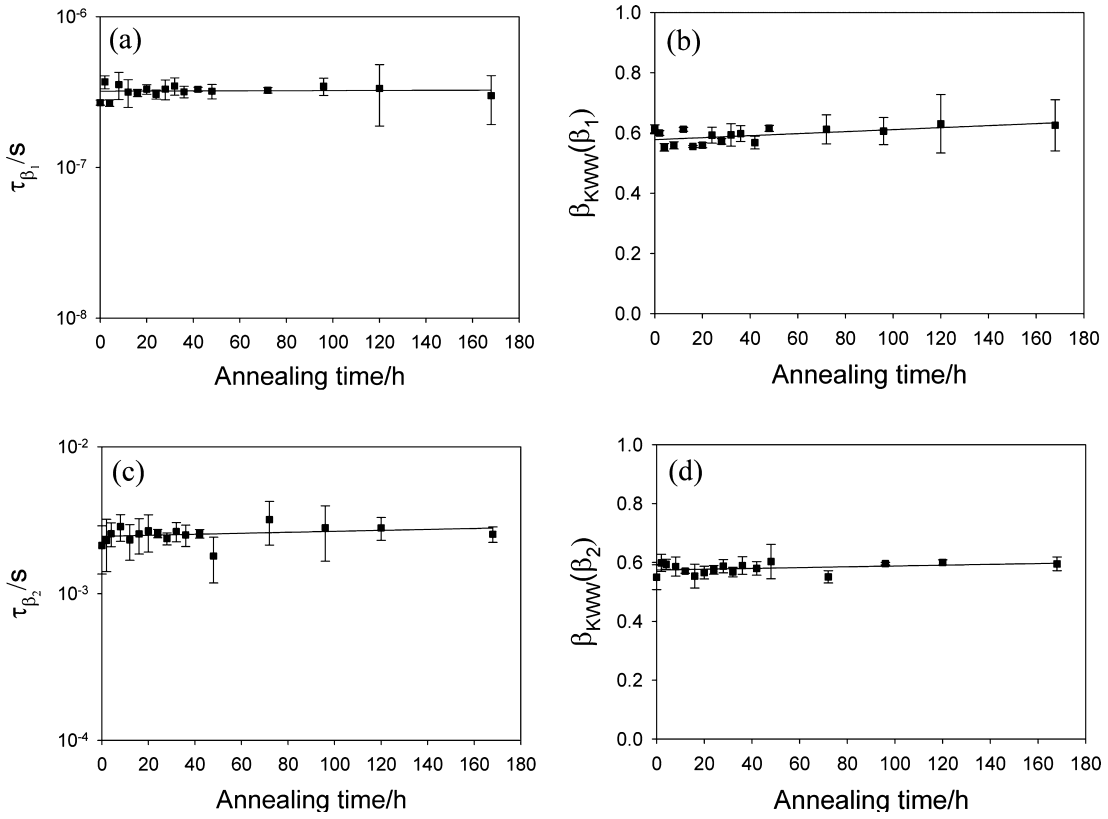

Figure 6. Plots of average relaxation times and β_{KWW} versus annealing time for β_1-relaxation (a and b) and β_2-relaxation (c and d) at 25 °C. Lines have been drawn to assist in visualizing the trends.

where τ is the mean molecular relaxation time and T is the temperature; τ_0, D, and T_0 are constants; τ_0 is the relaxation time of the unrestricted material, D is called the strength parameter, and T_0 is considered the zero mobility temperature (theoretical Kauzmann temperature). At sub-T_g temperatures, the observed relaxation times are shorter than the values predicted by the extrapolated VTF curve (from the supercooled region), indicating that the molecules are frozen into the nonequilibrium state. In other words, the time to reach the equilibrium state is longer than the time scale of observation/measurement.

The temperature dependence of α-relaxation time above the T_g was described well by the VTF model (Figure 5). At higher temperatures (>140 °C), since the α-relaxation peak was completely resolved from dc conductivity, the untransformed (i.e., raw) data was directly used to calculate the relaxation times. At lower temperatures (120−140 °C), the overlap of dc conductivity and relaxation necessitated the use of the Kramers−Kronig transformation. However, it is instructive to recognize that a single set of VTF parameters comprehensively described the relaxation behavior of trehalose over this entire temperature range (Figure 5). Since the temperature dependence of conductivity is expected to be different from that of primary relaxation, this is additional evidence that the relaxation peak obtained after Kramers−Kronig transformation is indeed due to structural relaxation of trehalose. The VTF parameters were τ_0 (relaxation time of the unrestricted material) = 1.5 × 10^{-9} s and T_0 (the zero mobility temperature) = 352.5 K. The strength parameter or the D-value, which is a measure of kinetic fragility, was ∼2.3. This was in good agreement with the reported value of 5.1 (based on DSC data) and is indicative of a very fragile glass former.[44] The calculated value of T_g using the VTF equation, assuming a relaxation time of 100 s, was ∼112 °C (indicated by an arrow in Figure 5). The validity of the VTF model was evident from the fact that the calorimetric T_g onset temperature was 117 °C. However, the measured α-relaxation time for amorphous trehalose at 117 °C was ∼0.22 s (Figure 5). This is another example of a system wherein the relaxation time at T_g is not 100 s.[6,47]

The average structural relaxation times obtained by us are different from the previously reported values.[24,30,31] These differences become quite pronounced at elevated temperatures (≥140 °C). As already discussed, there are differences in the α-relaxation time values reported by different groups. A similar observation has been made in the case of sucrose, a structural analogue of trehalose. The reported values of α-relaxation time differed by an order of magnitude in two studies.[6,25,48] Although the exact reason for such differences is not known, it is instructive to note that the relaxation time will be influenced by the presence (and concentration) of impurities including water. We were the only group to prepare amorphous trehalose by freeze-drying, a preparation method in which the sample is not subjected to elevated temperatures. We could not find information on the thermal stability of trehalose at temperatures close to its melting point. Several other sugars, including sucrose, are known to degrade around their melting temperature.[49,50]

As mentioned earlier, the excess wing was observed at temperatures <T_g. It became more noticeable as the temperature was decreased while it disappeared at temperatures >T_g. This is probably due to the α-relaxation showing stronger temperature dependence than the JG relaxation, with the former completely overshadowing the latter in the supercooled state. This is a common trait of α-relaxation. Kaminski et al.

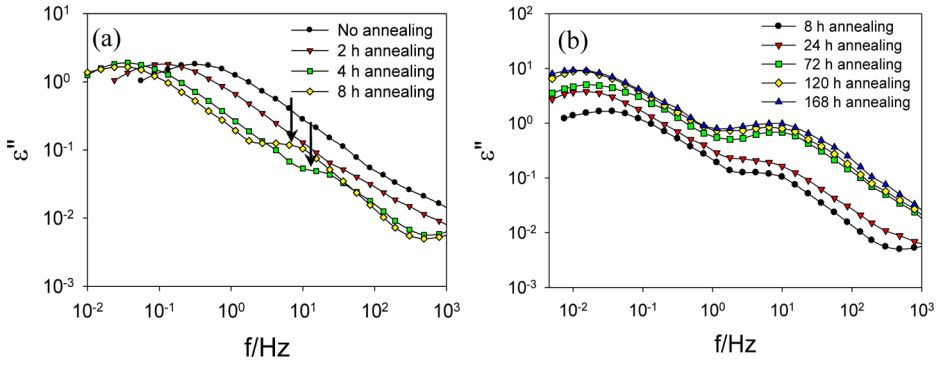

Figure 7. Isothermal dielectric loss spectra of amorphous trehalose annealed at 100 °C for different time periods. The frequency of maximum dielectric loss (f_{max}) is shown by arrows for β_3-relaxations in the left panel. The results from the left panel were presented earlier.[28]

used the Kramers–Kronig relation to characterize α-relaxation in trehalose.[25] Since they did not investigate the sub-T_g temperature range, the excess wing was not observed. We could not unambiguously investigate the temperature dependence of the excess wing due to overlap with the α-relaxation peak. In an effort to resolve the two relaxations and to fully characterize this local mobility, annealing was carried out.

Effect of Annealing on Molecular Mobility. *Effect of Annealing on Two Secondary Relaxations in Amorphous Trehalose.* In a previous study using thermally stimulated current (TSC) technique, trehalose was annealed at 100 and 90 °C for 4 and 7 h, respectively.[29] This had no effect on the secondary relaxation times. However, pharmaceutical amorphous materials are likely to be aged over time scales of days and months. Therefore, trehalose was annealed at 100 °C (17 °C < T_g) for 168 h. As shown in Figure 6 (panels a and c), there was no change in the average relaxation times of both β_1- and β_2-relaxations in trehalose annealed at 100 °C for 168 h. Thus, the relaxation time was unaffected by the reduction in free volume brought about by annealing. This is typical of motions which are intramolecular in origin and are unaffected by the motions of neighboring molecules. Although there was no change in the dielectric strength of β_1-relaxation, it decreased as a function of annealing for the slower β_2-relaxation (data not shown). This indicates that the number of molecules involved in the latter mobility decreased with sub-T_g annealing. As this mobility is intramolecular, decrease in free volume is not expected to have an effect on the magnitude of the rotational jump which has been implicated for this decrease in dielectric strength.[29] The distribution of different relaxations was also investigated as a function of annealing time. For this purpose, relaxation time distribution parameter from the Kohlrausch–Williams–Watts (KWW) equation, β_{KWW}, was calculated from the Havriliak–Negami peak width parameters β_{HN} and γ_{HN} using the empirical equation[51]

$$\beta_{KWW}^{1.23} = \beta_{HN}\gamma_{HN} \quad (5)$$

As is evident from Figure 6 (panels b and d), the distribution of the secondary relaxation times, and therefore heterogeneity, was unaffected by annealing. Thus, long-term annealing does not seem to affect these local relaxations in any way except for a decrease in the number of molecules involved in the slower β_2-relaxation.

Effect of Annealing on Global Molecular Mobility in Amorphous Trehalose. In order to investigate the effect of annealing on α-relaxation, the samples were annealed at 100 °C for different time periods and then subjected to DDS at the same temperature. A sharp increase was observed in the average α-relaxation time in the first 4 h of annealing (Figures 7 and 8).

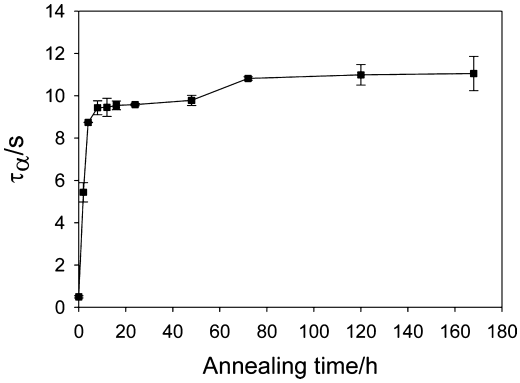

Figure 8. Plot of average α-relaxation time as a function of annealing time (n = 3). Both the annealing and the dielectric measurement were carried out at 100 °C.

Thereafter, the change in global mobility with annealing time was much less pronounced. This effect of annealing time on global mobility, although reported for the first time for trehalose, is in line with the behavior of other compounds.[44−46,52−54] Annealing is also expected to result in a moderate increase in the heterogeneity of distribution of structural relaxation times.[44,54] Due to the approximate nature of the Kramers–Kronig transformation, we did not consider the annealing-induced changes in the distribution of α-relaxation time. Annealing for a long time (up to 168 h) caused an increase in the dielectric strength of α-relaxation (Figure 7b). Since the structural relaxation time in the annealed samples (annealing time ≥2 h) was very long, the experiments had to be extended to the low-frequency range. This considerably increased the duration of the experiments. Therefore, in these samples, the measurement time was included in the total annealing time.

The samples annealed at 100 °C were also subjected to isothermal dielectric measurements (frequency sweeps) at several temperatures, over 90–170 °C. At any temperature of measurement below T_g, annealing initially resulted in a sharp increase in structural relaxation time. However, longer time periods of annealing had a much smaller effect on the relaxation time. As the temperature of measurement approached T_g, there was a progressive decrease in the magnitude of the overall annealing-induced change in relaxation time. Figure 9 shows the temperature dependence of average relaxation time for

dx.doi.org/10.1021/jp303317p | J. Phys. Chem. B 2012, 116, 11728–11736

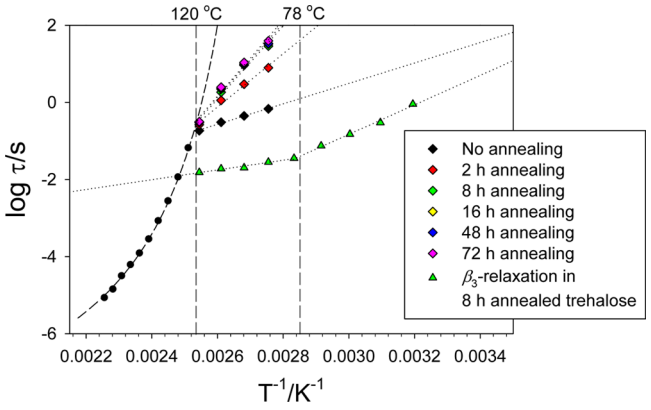

Figure 9. Effect of annealing on the temperature dependence of α-relaxation times. For the β_3-relaxation, the temperature dependence is shown only for the trehalose annealed for 8 h.

samples annealed for different time periods (0−72 h). In the sub-T_g range, annealing led to an increase in the activation energy for the structural relaxation. The effect on activation energy was also very pronounced in the first 8 h of annealing. It is evident that, with annealing, the glassy trehalose is moving toward the extrapolated VTF line which represents "equilibrium" behavior.

At temperatures below T_g, the structural relaxation times are of the order of minutes or hours and dielectric measurements in the frequency domain become very time-consuming. Earlier studies have demonstrated this annealing effect using time domain methods (both dielectric as well as TSC techniques).[45,46,52,53] However, the fast relaxation dynamics in amorphous trehalose at temperatures even below T_g enabled us to observe this behavior using dielectric spectroscopy in the frequency domain.

Effect of Annealing on Excess Wing. In an earlier report, we have shown the effect of short annealing times (up to 8 h) on the excess wing in the dielectric spectrum of amorphous trehalose.[28] On annealing, there was a shift in α-relaxation peak to lower frequencies leading to the resolution of this underlying mode of mobility (β_3-relaxation). The most pronounced effect on β_3-relaxation time was observed in the first 8 h of annealing (Figure 7a). During this time, the frequency of maximum loss appeared to shift to lower values (pointed out in Figure 7a), although there was still a considerable overlap with α-relaxation. On annealing for >8 h, the relaxation time appeared to be unaffected (Figure 7b). However, these longer annealing times caused an increase in dielectric strength, as was also observed with α-relaxation (Figure 7b).

Thus, the effect of annealing on β_3-relaxation is qualitatively similar to that on α-relaxation. We also reported a good agreement between the measured average relaxation time of this mobility and the calculated independent relaxation time based on the coupling model.[28] All these observations indicate that this excess wing is the high-frequency flank of the Johari−Goldstein (JG) relaxation hidden under the primary relaxation.

As already mentioned, the excess wing developed into an unresolved relaxation peak upon annealing. In trehalose annealed for 8 h, we modeled the peak and obtained the relaxation time and shape parameters at different temperatures. The relaxation time did not exhibit a linear temperature dependence (Figure 9). However, it could be described by two Arrhenius models intersecting at ∼78 °C. This change in temperature dependence is analogous to the glass transition temperature in α-relaxation, though its physical significance is unknown.

CONCLUSIONS

Using dielectric spectroscopy, molecular mobility in amorphous trehalose was characterized. Two secondary relaxations were detected at temperatures $\ll T_g$. At temperatures close to T_g, characterization of α-relaxation was possible only after subtraction of dc conductivity. The various sources of artifacts, both instrumental and sample related, that could lead to a conductivity peak in this region were considered. Diagnostic tests were performed to ensure that this peak was due to primary relaxation of trehalose and not conductivity. Long-term sub-T_g annealing revealed a pronounced shift of the α-relaxation to lower frequencies leading to the resolution of an excess wing into a relaxation peak which was attributed to the Johari−Goldstein process. The temperature dependence of this local mobility could be described by two Arrhenius models intersecting at ∼78 °C. Annealing did not have any effect on the relaxation time of the two other β-relaxations.

AUTHOR INFORMATION

Corresponding Author

*Phone: 612-624-9626. Fax: 612-626-2125. E-mail: surya001@umn.edu.

Notes

The authors declare no competing financial interest.

ACKNOWLEDGMENTS

We thank Brad L. Givot (3M, St. Paul, MN) for all his help and support during the course of the project and 3M (St. Paul, MN) for providing us generous access to the dielectric spectrometer. Marcus T. Cicerone (NIST, Gaithersburg, MD), Khushboo Kothari, and Vishard Ragoonanan are thanked for their insightful comments. Partial support was provided by the William and Mildred Peters Endowment Fund.

REFERENCES

(1) Crowe, J. H.; Crowe, L. M.; Carpenter, J. F.; Aurell Wistrom, C. *Biochem. J.* **1987**, *242*, 1−10.
(2) Leslie, S. B.; Israeli, E.; Lighthart, B.; Crowe, J. H.; Crowe, L. M. *Appl. Environ. Microbiol.* **1995**, *61*, 3592−3597.
(3) Sundaramurthi, P.; Suryanarayanan, R. *J. Phys. Chem. Lett.* **2010**, *1*, 510−514.
(4) Sundaramurthi, P.; Patapoff, T. W.; Suryanarayanan, R. *Pharm. Res.* **2010**, *27*, 2374−2383.
(5) Crowe, J. H.; Carpenter, J. F.; Crowe, L. M. *Annu. Rev. Physiol.* **1998**, *60*, 73−103.
(6) Bhugra, C.; Rambhatla, S.; Bakri, A.; Duddu, S. P.; Miller, D. P.; Pikal, M. J.; Lechuga-Ballesteros, D. *J. Pharm. Sci.* **2007**, *96*, 1258−1269.
(7) Bhugra, C.; Shmeis, R.; Krill, S. L.; Pikal, M. J. *J. Pharm. Sci.* **2008**, *97*, 455−472.
(8) Aso, Y.; Yoshioka, S.; Kojima, S. *J. Pharm. Sci.* **2004**, *93*, 384−391.
(9) Sixou, B.; Faivre, A.; David, L.; Vigier, G. *Mol. Phys.* **2001**, *99*, 1845−1850.
(10) Paluch, M.; Pawlus, S.; Hensel-Bielowka, S.; Kaminski, K.; Psurek, T.; Rzoska, S. J.; Ziolo, J.; Roland, C. M. *Phys. Rev. B* **2005**, *72*, 224205.
(11) Johari, G. P.; Goldstein, M. *J. Chem. Phys.* **1970**, *53*, 2372−2388.
(12) Vyazovkin, S.; Dranca, I. *J. Phys. Chem. B* **2007**, *111*, 7283−7287.
(13) Alie, J.; Menegotto, J.; Cardon, P.; Duplaa, H.; Caron, A.; Lacabanne, C.; Bauer, M. *J. Pharm. Sci.* **2004**, *93*, 218−233.

(14) Hikima, T.; Adachi, Y.; Hanaya, M.; Oguni, M. *Phys. Rev. B* **1995**, *52*, 3900−3908.
(15) Hikima, T.; Hanaya, M.; Oguni, M. *J. Mol. Struct.* **1999**, *479*, 245−250.
(16) Johari, G. P. *J. Non-Cryst. Solids* **2002**, *307*−*310*, 317−325.
(17) Vij, J. K.; Power, G. *J. Non-Cryst. Solids* **2011**, *357*, 783−792.
(18) Ngai, K. L. *J. Phys.: Condens. Matter* **2003**, *15*, S1107−S1125.
(19) Ngai, K. L. *J. Chem. Phys.* **1998**, *109*, 6982−6994.
(20) Weuts, I.; Kempen, D.; Six, K.; Peeters, J.; Verreck, G.; Brewster, M.; Van den Mooter, G. *Int. J. Pharm.* **2003**, *259*, 17−25.
(21) Surana, R.; Pyne, A.; Rani, M.; Suryanarayanan, R. *Thermochim. Acta* **2005**, *433*, 173−182.
(22) Andronis, V.; Zografi, G. *Pharm. Res.* **1997**, *14*, 410−414.
(23) Aso, Y.; Yoshioka, S.; Kojima, S. *J. Pharm. Sci.* **2000**, *89*, 408−416.
(24) De Gusseme, A.; Carpentier, L.; Willart, J. F.; Descamps, M. *J. Phys. Chem. B* **2003**, *107*, 10879−10886.
(25) Kaminski, K.; Kaminska, E.; Wlodarczyk, P.; Pawlus, S.; Kimla, D.; Kasprzycka, A.; Paluch, M.; Ziolo, J.; Szeja, W.; Ngai, K. L. *J. Phys. Chem. B* **2008**, *112*, 12816−12823.
(26) Cummins, H. Z.; Zhang, H.; Oh, J.; Seo, J.-A.; Kim, H. K.; Hwang, Y.-H.; Yang, Y. S.; Yu, Y. S.; Inn, Y. *J. Non-Cryst. Solids* **2006**, *352*, 4464−4474.
(27) Bhardwaj, S. P.; Givot, B. L.; Suryanarayanan, R. *AAPS J.* **2010**, *12*, S2.
(28) Bhardwaj, S. P.; Suryanarayanan, R. *Mol. Pharm.* **2011**, *8*, 1416−1422.
(29) Moura Ramos, J. J.; Pinto, S. S.; Diogo, H. P. *ChemPhysChem* **2007**, *8*, 2391−2396.
(30) Kwon, H.; Seo, J.; Kim, H. K.; Hwang, Y. *J. Chem. Phys.* **2011**, *134*, 014508.
(31) Kaminski, K.; Wlodarczyk, P.; Paluch, M. *J. Chem. Phys.* **2011**, *135*, 167102.
(32) Lynch, A. C. *Proc. IEE* **1971**, *118*, 244−246.
(33) Richert, R. *J. Chem. Phys.* **2010**, *133*, 074502.
(34) Richert, R.; Agapov, A.; Sokolov, A. P. *J. Chem. Phys.* **2011**, *134*, 104508.
(35) Richert, R. *Eur. Phys. J. B* **2009**, *68*, 197−200.
(36) Wübbenhorst, M.; Turnhout, J. *J. Non-Cryst. Solids* **2002**, *305*, 40−49.
(37) Kaminski, K.; Adrjanowicz, K.; Paluch, M.; Kaminski, E. *Phys. Rev. E* **2011**, *83*, 061502.
(38) Schneider, U.; Brand, R.; Lunkenheimer, P.; Loidl, A. *Phys. Rev. Lett.* **2000**, *84*, 5560−5563.
(39) Lunkenheimer, P.; Wehn, R.; Riegger, T.; Loidl, A. *J. Non-Cryst. Solids* **2002**, *307*−*310*, 336−344.
(40) Crowe, L. M.; Reid, D. S.; Crowe, J. H. *Biophys. J.* **1996**, *71*, 2087−2093.
(41) Ding, S.-P.; Fan, J.; Green, J. L.; Lu, Q.; Sanchez, E.; Angell, C. A. *J. Therm. Anal.* **1996**, *47*, 1391−1405.
(42) Miller, D. P.; Pablo, J. J. d.; Corte, H. *Pharm. Res.* **1997**, *14*, 578−590.
(43) Surana, R.; Pyne, A.; Suryanarayanan, R. *Pharm. Res.* **2004**, *21*, 1167−1176.
(44) Shamblin, S. L.; Tang, X.; Chang, L.; Hancock, B. C.; Pikal, M. J. *J. Phys. Chem. B* **1999**, *103*, 4113−4121.
(45) Schlosser, E.; Schönhals, A. *Polymer* **1991**, *32*, 2135−2140.
(46) Goitiandia, L.; Alegría, A. *J. Non-Cryst. Solids* **2001**, *287*, 237−241.
(47) Bhattacharya, S.; Suryanarayanan, R. *Pharm. Res.* **2011**, *28*, 2191−2203.
(48) Kaminski, K.; Kaminska, E.; Hensel-Bielowka, S.; Chelmecka, E.; Paluch, M.; Ziolo, J.; Wlodarczyk, P.; Ngai, K. L. *J. Phys. Chem. B* **2008**, *112*, 7662−7668.
(49) Hurtta, M.; Pitkänen, I.; Knuutinen, J. *Carbohydr. Res.* **2004**, *339*, 2267−2273.
(50) Richards, G. N.; Shafizadeh, F. *Aust. J. Chem.* **1978**, *31*, 1825−1832.
(51) Alvarez, F.; Alegría, A.; Colmenero, J. *Phys. Rev. B* **1991**, *44*, 7306−7312.
(52) Alegría, A.; Goitiandia, L.; Tellería, I.; Colmenero, J. *J. Non-Cryst. Solids* **1991**, *131*−*133*, 457−461.
(53) Alegría, A.; Goitiandía, L.; Tellería, I.; Colmenero, J. *Macromolecules* **1997**, *30*, 3881−3887.
(54) Mao, C.; Chamarthy, S. P.; Pinal, R. *Pharm. Res.* **2006**, *23*, 1906−1917.
(55) Kaminski, K.; Adrjanowicz, K.; Zakowiecki, D.; Kaminska, E.; Wlodarczyk, P.; Paluch, M.; Pilch, J.; Tarnacka, M. *Mol. Pharm.* **2012**, *9*, 1559−1569.

■ NOTE ADDED IN PROOF

While this paper was under review, Kaminski et al. published their work outlining the dielectric properties of sucrose and trehalose.[55] In this paper, they have questioned some of our conclusions in an earlier paper relating to the molecular mobility of trehalose.[28] We believe that we have comprehensively responded to these concerns in the current manuscript, specifically through Figure 3 and the associated text.